Folic Acid-modified Lysozyme-protected Gold Nanoclusters as Anti-inflammatory Nanomedicine for Gout Flares

Jiachen Sun
First Affiliated Hospital of Jinzhou Medical University
Pengfei Zhuang
First Affiliated Hospital of Jinzhou Medical University
Shan Wen
First Affiliated Hospital of Jinzhou Medical University
Minghao Ge
First Affiliated Hospital of Jinzhou Medical University
Zipeng Zhou
First Affiliated Hospital of Jinzhou Medical University
Dan Li
First Affiliated Hospital of Jinzhou Medical University
Chang Liu
First Affiliated Hospital of Jinzhou Medical University
Xifan Mei (meixifan@jzmu.edu.cn)
First Affiliated Hospital of Jinzhou Medical University https://orcid.org/0000-0003-3698-0525

Research

Keywords: Gout flare, Anti-inflammatory effects, nanomedicine, orgnic drug-free, Gold Nanoclusters, Side effects

Posted Date: October 25th, 2021

DOI: https://doi.org/10.21203/rs.3.rs-993031/v1

Abstract

Background

Gout normally occurs when excess urate crystals accumulate in the joints that induce inflammation. The inflammations further result in gout flares, causing serious pain. Some anti-inflammatory drugs can relieve pain, but they have significantly toxic and side effects. Nanomedicines offer opportunities to reduce various side effects but are mostly based on the delivery of additional organic drugs, which adds complexity and may cause other health problems including the bioaccumulation risk. We developed folic acid (FA)-modified lysozyme (Lys)-protected gold nanoclusters (AuNCs) (i. e., FLA) by a one-pot method, and FLA is developed as an anti-inflammatory drug in the treatment of acute attacks of gout flares at high monosodium urate (MSU) levels.

Methods

The morphological changes of the cells caused by FLA were studied by Transmission electron microscopy (TEM) and fluorescence microscopy. Western blotting was conducted to understand the inflammation factors. AutoDock Vina was used for molecular docking of FLA to evaluate the binding mode of the ligand and the interaction in the active site.

Results

This nanomedicine significantly reduced the inflammation of gout flares. In addition, the oxidative stress level was found to decrease to normal values by FLA based on the evaluation of reactive oxygen species (ROS). By injecting FLA into the gout rat model, inflammation was remarkably reduced during gout attacks, and cartilage destruction was significantly relieved. The biosafety of this nanomedicine is confirmed by insignificant cytotoxicity and no bioaccumulation-induced organ change.

Conclusion

Compared with traditional nano-delivery systems, this organic drug-free nanomedicine exhibits exciting therapeutic efficiency against gout flares, which will have considerable prospects in the clinic.

Introduction

Gout is a metabolic disease that occurs due to purine metabolism disorders and increased blood uric acid. The most common symptom of gout flares is a more serious pain, stiffness, and swelling in the joints than common arthritis [1] [2]. Current clinical management of gout flares relies on colchicine, non-steroidal anti-inflammatory drugs, glucocorticoids, and adrenocorticotropic hormones [1, 3]. Unfortunately, these treatments have caused various problems including irritability, mood disorders, increased blood glucose levels, immunosuppression, and fluid retention [4]. On the other hand, due to the unsatisfactory therapeutic efficiency, the need for large doses and frequent administration causes

difficulties for long-term treatment [5]. There is an urgent need for safer and more effective drugs to treat gout flares.

In recent years, nanomedicines reduce the side effects for treating many diseases, and dosage is also reduced because of the larger active area. Several nano-drug deliver antiphlogistic durgs were used for treating arthritis [6–8], showing more satisfied biosafety and efficiency. Although significant improvement has been made, additional antiphlogistic durgs are still involved [9]. Several nano agents were directly applied for uric acid reduction without loading additional antiphlogistic durgs, but the inflammatory problems were hardly solved [10, 11]. The limited efficiency of these nanomedicines might be attributed to their therapeutic strategies, which only focused on reducing MSU [12]. During the acute attack of gout flares, it is not suggested to use uric acid lowering drugs. Not only does it have insignificant anti-inflammatory and analgesic effects, but also causes the blood uric acid to drop too quickly, which promotes the dissolution of tophi in the joints, forming insoluble crystals and aggravating inflammation. Uric acid-lowering treatment can be started only after the acute symptoms are relieved (≥2 weeks). Thus, We are trying to establish a method that can deal with acute attacks of gout flares, even in the case of high uric acid, which can still reduce inflammation.

AuNCs have been widely studied as antiphlogistic durg-free nanomedicines because of their biosafety, insignificant bioaccumulation in the body, and antioxidant effects [13, 14] [15]. AuNCs have been designed as a probe for uric acid, which is related to gout [16], indicating they may have various target effects for this disease. Herein, we developed FLA as antiphlogistic durg-free nanomedicine for the treatment of gout flares. This nanomedicine evokes immune function and shows excellent anti-inflammatory effects on rat models with gout flares [17–19]. FLA also enables the joint swelling of gout rats to recover efficiently. To the best of our knowledge, this is the first study to use AuNCs to successfully relieve the inflammations and other symptoms for rats with gout flares.

Results And Discussion

Characterization of FLA

Based on a similar mechanism [22], the scheme for the synthesis of FLA (Fig. 1A) and the mechanism is proposed for the construction of FLA (Fig. 1B). Initially, Lys and Au(I), Au(I) binds to the 1-N of His15 of Lys. The free Au(I) in the mother liquor continuously diffuses into the Lys and then disproportionates into Au(0) and Au(III) in the crystal. Au(0) is further assembled as clusters, and Au(III) translocates and recombines to other sites in Lys. AutoDock Vina was used for molecular docking of FLA to evaluate the binding mode of the ligand and the interaction in the active site. PyMol has been used to generate a 3D pose of the recognized ligand that binds to the active site of LA, and its binding energy is 7.0 kcal/mol. Folate and amino acids form conventional hydrogen bonds (HB) GLU-35, ASN-59, TRP-62, ALA-107, ALA-110, and ASN-113. In addition, it forms π-anion interactions with ASP-52, and π-sigma and π-alkyl interactions with ALA-110. According to the molecular docking theory, folic acid molecules can be perfectly combined with AuNCs.

The AuNCs, FLA, and AuNPs were characterized with TEM (Fig. 1C). All of the AuNCs are well dispersed and the size was about 2.88 nm. Also, aggregation of the AuNCs cannot be found from the TEM images. Therefore, we assume that the use of Lys as a stabilizer can inhibit the formation of larger particles. The FA enabled AuNCs to grow to 4.5 nm in diameter. However, the AuNPs that mixed with Lys were 16 nm in diameter. Because of the small size and the biocompatible surface, these materials would be transferred into human cells. The alteration in the charge of the particles in the microenvironment and the attachment of FA on the surface of AuNCs may perturb the electron density into the metal nanoparticle and consequently change the inner interaction and the size.

Targeted Therapy for gout

Normal RAW 264.7 cells were cultured with FLA (100 μM) containing medium and treated with LPS and MSU crystals for 24 h. Cells were labeled with FITC fluorescent (green) clusters and the location of the cells was visualized by staining the nucleus with DAPI (blue) and the cytoskeleton with Tubulin (red). It was found that RAW 264.7 cells could effectively take up FLA (Fig. 2A). the same treatment was followed by TEM observation of the cells and the results were the same as for confocal microscopy. RAW 264.7 cells could effectively take up FLA (Fig. 2B). The fluorescent agent FITC was loaded into FLA and its distribution in vivo was studied (Fig. 2C). We could observe that the fluorescent signal of FLA in the FLA group accumulated at the kidney before 8 h and was rapidly removed from the body after 8h, indicating that FLA was rapidly cleared in vivo. However, in the FLA+Model group, FLA aggregated at the kidney and ankle at 2 h. This suggests that FLA enhances the accumulation of fluorescence in the ankle joint. It was noted that FLA aggregated in the kidney in both the FLA and FLA+Model groups, representing that FLA is excreted from the body mainly through the kidneys (Fig. 2D-E). FLA can target the swollen and inflamed ankle joints of rats and is phagocytosed by macrophages. Then, they are cleaned by the kidneys. Therefore, FLA are promising to show therapeutic effects towards gout and biosafety.

Anti-inflammation in vitro

The FLA on MSU-induced inflammatory response in vitro was observed under confocal microscopy. We found that FLA inhibited the production of IL-1β, a key cytokine for gout inflammation that causes gout flares, and had a stronger effect than treatment with Lys and AuNCs alone (Fig. 3A-B, D-E) Since gout is a dual-signal-driven disease. NLRP3 inflammatory vesicles are responsible for IL-1β maturation, and another signal upregulates IL-1β transcription and pro-IL-1β synthesis [1, 25]. Therefore, the effects of FLA on NACHT, LRR, and PYD domain-containing protein 3(NLRP3) inflammatory vesicles, as well as the Toll-like receptors (TLR) signaling pathway, was examined. Western blot analysis revealed that FLA significantly reduced the protein levels of Caspase1(Fig. 3F), ASC(Fig. 3G), NF-κB (Fig. 3K) and was superior to Lys and AuNCs alone, suggesting that Lys acts as a shell ligand to enhance the efficacy of gold nanoclusters. At the same time, we found that FLA also decreased the protein levels of IL-6(Fig. 3H), TNF-α(Fig. 3I), and COX-2 (Fig. 3J). This may be related to the initiation of IL-1β signaling, leading to the production and secretion of pro-inflammatory mediators, and the up-regulation of pro-inflammatory cytokines through the binding of activated NF-κB to the promoter region of target genes [32–34]. As a

result, it is concluded FLA can effectively inhibit the production of IL-1β and reduce the occurrence and expansion of gout flares. FLA also has promising therapeutic effects on common diseases that respond to IL-1β neutralization such as type 2 diabetes, heart failure, recurrent pericarditis, rheumatoid arthritis, and smoldering myeloma [35]. Thus, the administration of FLA can exhibit comprehensive therapeutic effects for gout patients.

Antioxidant effects

MSU crystals can activate NLRP3 inflammatory vesicles and thus increase IL-1β release via ROS [36]. To elucidate the mitigating effect of FLA on gout inflammation. We investigated the effect of FLA on oxidative stress using Raw 264.7 cells. We treated each group of RAW 264.7 cells with 100 μM FLA for 24 h and observed them with TEM, and found that the mitochondria in the sham group had normal morphology and clear mitochondrial ridges. The mitochondria in the FLA group showed significant improvement compared to the Model group (Fig. 4B). Also for exogenous ROS that was studied, Raw 264.7 was exposed to 20 μM H$_2$O$_2$ for up to 30 minutes and incubated in the presence or absence of FLA, Lys, AuNPs for 4 h. The production of ROS was observed by confocal fluorescence microscopy. A significant reduction of ROS in the FLA group could be found (Fig. 4C). The SOD-like enzyme activity, GSH level, and MDA level can reflect the antioxidant effects. The FLA group showed higher SOD-like activity than the Model, AuNPs, and Lys groups (Fig. 4D). The MDA content showed an opposite trend: the FLA group showed significantly lower MDA content than the Model, AuNPs, and Lys groups (Fig. 4E). Amount of GSH analysis showed that the FLA group had significantly higher GSH content than the Model, AuNPs, Lys group (Fig. 4F). These changes were attributed to the enhanced ability of FLA to resist oxidative stress after a gout attack. In addition, there are several other possibilities for FLA to inhibit ROS. The first is to inhibit the NF-κB inflammatory factor leading to a decrease in the level of nitric oxide synthase (INOS) induced by downstream inflammatory factors, thereby reducing the production of free radicals such as NO, thereby reducing the level of ROS [37, 38]. Secondly, the level of ROS may be reduced by regulating nuclear factor E2-related factor 2 transcription factor (Nrf2) [39, 40], which may also be related to the buffering of oxygen radicals [41]. This suggests that FLA act as ROS scavengers in acute attacks of gout.

Anti-inflammatory effects in vivo

The injection of MSU crystals (0.5 mg/10 ml) into the ankle of SD rats can increase the protein level of the pro-inflammatory cytokine IL-1β in the tissues around the ankle [25, 30]. Western blot analysis showed that FLA significantly reduced the protein levels of IL-1β (Fig. 5A), Caspase1 (Fig. 5D), ASC (Fig. 5E), NF-κb (Fig. 5K), COX-2 (Fig. 5G), IL-6 (Fig. 5F), and TNF-α (Fig. 5I). Its anti-inflammatory effect was consistent with the results of in vivo and in vitro experiments. COX-2 is a key enzyme that converts cell membrane arachidonic acid into inflammatory mediator prostaglandin 2 (PGE2), which is an important pain mediator. It plays an important role in the noxious stimulation of gout. Due to the down-regulation of COX-2, we assume that the protein level of PGE 2 will also down-regulate and have an analgesic effect on

gout flares [42]. FLA effectively inhibits pro-inflammatory up-regulated cytokines, indicating the therapeutic effects on the acute attack of gout flares.

In vivo recovery of gout flares

The circumference of 1 cm above the thinnest point of the rat's ankle joint was measured to assess the degree of edema in the rat's ankle joint (Fig. 6A). By observing the injection of different concentrations of FLA with gout rats, we found that at 24h, the swelling reached its highest peak and was most effectively inhibited by FLA. According to the method to assess the inflammation and dysfunction index of rats, the inflammation and dysfunction index of the ankle of gout rats peaked at 24 with complete swelling and lameness on the swollen side. FLA (20 mg/kg) significantly improved their inflammation and dysfunction index (Fig. 6B-E). After 24 h, we selected the ankle of the rat for HE staining of the SD section and found it. In the gout model group, the joint cavity became smaller, with fluid exudation and inflammatory cell infiltration. The cartilage layer becomes thinner, and the chondrocytes have vacuole-like changes and degenerative necrosis. There were fewer lesions in the treatment group. This is consistent with the hematoxylin and eosin-stained sections of the ankle joint (Fig. 6F) that FLA can reduce the ankle swelling caused by MSU. The administration of FLA also reduces tissue destruction caused by inflammation.

Biosafety plays an important role in determining whether nanomedicines can be used to treat diseases. Herein, Raw 264.7 cells were used to test cell viability by the MTT method. Cells were studied in the presence of FLA at 0 to 320 μM. No dose-response pattern was seen in Raw 264.7 at concentrations less than 320 μM. The cell viability of the cells was almost 100% (Fig. S1A). To study the toxicity of FLA in vivo. The organs were studied by histopathological analysis after injection of different concentrations of FLA (5, 10, 20 mg/kg) on the first day and 14th day. Microscopically, myocardial fibers were seen to be interwoven and arranged, with nuclear ellipses located centrally and capillaries abundant between myofibers. Hepatocytes were closely arranged, binucleated cells were common, and connective tissue content was low. The splenic white and red marrow structures were clear, and there was no significant increase in lymphoid tissue. The alveolar structure was intact and the interstitium was not fibrotic. There was no swelling of the renal nodules, the size of the renal capsule was normal, and the cubic renal tubule cells were not diseased. In addition, there was no significant structural difference between the material group and the control group (Fig. S1C-D). All these results indicate that FLA are safe for the treatment of gout flares in vivo and in vitro.

Conclusions

This study demonstrates a new anti-inflammation strategy for the fast therapy of gout flares using (FLA). FLA directly reduces the inflammation of the rat with gout flares without additional antiphlogistic durgs, which quickly repairs joints and other functions. This opens an avenue for relieving the serious pain for gout patients using antiphlogistic durg-free nanomedicines, which is promising for long-term use.

Methods

Materials and Instruments

$HAuCl_4$, Lys, citrate sodium was obtained from Sigma Aldrich. The dialysis tube (MWCO 6000) was supplied by Spectrum. All other reagents were of analytical grades used as received without further purification. Ultrapure water (18.0 MΩ, Millipore) was used for all the experiments. Elemental analyses were performed by inductively coupled plasma mass spectrometry (ICP-MS) (Thermo). Microscopic images were investigated with a Tecnai G220 transmission electron microscope (TEM, 200 kV) (FEI, USA). Zeta potential was studied by Malvern sizer 3000. Fluorescence images were taken with Leica TCS SP5 II.

Preparation of FLA

Synthesis of AuNCs (LA) 2.5 mL of Lysozyme (Lys) solution (15 mg/mL) was mixed with 2.5 mL of aqueous $HAuCl_4$ (5 mM) solution in a 50 mL vial. The mixture was stirring for 5 minutes. Then, 100 μL of 100 mM NaOH solution was introduced with continuously stirring until transparent. Then, the vial was transferred to a 37 °C water bath and kept at this temperature for 24 h. The samples were purified by a dialysis tube (MWCO 6000) for more than 24 h before use.

Synthesis of FLA 10 ml of dimethyl sulfoxide (DMSO) was loaded in a 50 ml round bottom flask. FA (0.16 g, 0.36 mmol) was added into the flask and stirred until dissolved. 1-ethyl-3-(-3-dimethylaminopropyl) carbodiimide (EDC) and N-(3-Dimethylaminopropyl)-N'-ethyl carbodiimide hydrochloride (NHS) with a ratio of (Folic acid: EDC: NHS=1: 1: 1) were added to the reaction and stirred for 20 h in the dark. Finally, AuNCs (2.5 mmol) were added to the mixture and further stirred for 16 h. The samples were purified by a dialysis tube (MWCO 6000) for more than 24 h before use.

Synthesis of AuNPs by the adsorption of Lys The synthesis of the citrate stabilized AuNPs (Gold nanoparticles) was following a method described by the reference [20]. Next, 2.5 mL of Lys solution (15 mg/mL) was mixed with 2.5 mL of AuNPs (5 mM) (the concentration is corresponding to the Au element).

Molecular Dynamics

The molecular docking was performed using AutoDock Vina [21] to reveal the binding affinity and interactions of FA with the surface of AuNCs (PDB ID: 7BV2) [22]. FA was docked on the site using the optimized grid box and nine poses were generated. All of the docking results were ranked by energy and the lowest binding energy was selected. The docking interactions of FLA and FA were visualized and analyzed using PyMol [23].

Animals and Models

Adult SD rats (half male and half female, weight 180-220 g, 10-12 weeks) were purchased from Nanjing Institute of Biomedical Research, Nanjing University. The experimental procedures were approved by the Animal Protection and Use Committee of Jinzhou Medical University. ethical committee

number:2021101.The animal data were reported following the ARRIVE 2.0 guidelines[24]. All rats were placed in standard cages in the SPF Laboratory Animal Center of Jinzhou Medical University. They had access to free food and water on a 12/12-hour day/night cycle and at the appropriate temperature. The animals were allowed to acclimatize to these conditions for at least 2 days before starting the experiments. For each group of experiments, animals were matched by age and body weight, and all procedures were performed at 1% sodium pentobarbital 50 mg/kg, with an intra-ankle injection of MSU crystal 1 suspension (1.25 mg/100μl) [25-28].

Cell preparation and stimulation

Raw 264.7 was kept in moist 5% CO_2 at 37°C in Dulbecco supplemented with 10% (modified Eagle's medium v/v streptomycin (U/ml)) FBS, penicillin (100 U/ml) (Gibco, Grand Island, NY, USA) and. The cells were inoculated in cell dishes overnight and the medium was changed to serum-free medium the next morning, then the cells were treated with LPS (1 μg/ml) with or without Lys, AuNPs, and FLA. The treatment lasted for 12 h and was stimulated with MSU crystals (200 μg/ml) for 12 h. Analysis of cell extracts and precipitated supernatants by immunoblotting.

MSU crystal preparation

In 45 ml of 0.03 M NaOH solution (pH 7.5), 250 mg of uric acid (Solarbio, Beijing, China) was heated to boil. The solution was filtered and 1 ml of 5 M NaCl was added to accelerate crystal formation. The solution was gently stirred at room temperature for 24 h or until a milky white precipitate formed. The crystals were kept sterile, washed with ethanol and acetone, and dried at room temperature. The MSU crystals were resuspended in PBS at a concentration of 24 mg/ml, sonicated, and used under sterile conditions. MSU crystal preparations are evaluated with specific Limulus reagent (Maclean's, Shanghai, China) and are endotoxin-free [29, 30].

Cell viability

Cell viability was studied based on cell counting MTT assay analysis of Raw 264.7. First, cells were inoculated in 96-well plates at a density of 4×10^3 per well and incubated overnight. In addition, two types of cells were exposed to the medium for 24 h in the absence (control) and the presence of 5, 10, 20, 40, 80, 160, and 320 μM FLA, respectively. Next, the culture medium was discarded and washed carefully with PBS 2-3 times. Then 20 μL of MTT solution (5 mg/mL) was added to each well and the plates were incubated at 37°C, 5% CO_2 for 4 h until the purple methanogenic product appeared. After careful removal of the medium, the purple product is dissolved in 150 μL of dimethyl sulfoxide (DMSO). Cell viability was studied by recording the absorbance at 450 nm with an enzyme marker (n = 5/group).

Western blot

Proteins were extracted from macrophages and ankle joint homogenates with Radio Immunoprecipitation Assay (RIPA) buffer, measured by BCA protein assay (Solarbro, Beijing, China), sampled by SDS-PAGE,

and loaded with 30-60 μg protein, then electrophoresed and transferred to polyvinylidene fluoride membrane (Millipore Corp., Bedford, Massachusetts). The membrane was blocked with 5% bovine serum albumin for 2 h at room temperature, probe with primary antibody (Invitrogen, Waltham, MA) overnight at 4°C, and then incubated with HRP-conjugated secondary antibody (Invitrogen, Waltham, MA) 2 h. The main antibodies used were IL-1β, Caspase1, ASC, Nf-κb, Cox-2, TNF-α, β-Actin, and then the filter membrane was developed with an enhanced chemiluminescence reagent (Tanon, Shanghai, China). And through the Tanon 5500 gel imaging system (Tanon, Shanghai, China) to visualize the signal (n = 3 / group).

Immunofluorescent dual-labeling staining

RAW 264.7 cells in each group were incubated for a certain period and washed with PBS three times. Then, these cells were fixed with 4% PFA for 30 minutes. Subsequently, the cells were washed 3 times with PBS, punched with Triton X-100 (0.3%) for 15 minutes, washed 3 times with PBS, and then blocked with 5% goat serum for 2 h. Then, these cells were incubated with primary IL-1β antibody and β-tubulin antibody (Invitrogen, Waltham, MA) in a culture medium at 4 °C overnight. Then the cells were washed 3 times with PBS. Subsequently, these cells were incubated with secondary antibodies (Alexa Fluor 546 labeled anti-rabbit IgG) and anti-mouse IgG (Alexa Fluor 488 labeled anti-mouse IgG) (Invitrogen, Waltham, MA) for 2 h and washed for 3 Secondly by PBS. Finally, the cells were stained with DAPI for 15 minutes. Similarly, RAW 264.7 cells were cultured with or without FLA (100 μM) medium, and FITC was added for 24 h. Then, the cells were fixed with 4% PFA for 30 minutes. Subsequently, the cells were washed 3 times with PBS. The cells were incubated overnight at 4°C in a medium containing an anti-β-tubulin antibody. Next, these cells were incubated with the corresponding secondary antibodies for 2 h, washed 3 times, and stained with DAPI for 15 minutes. The cells were then observed through a single-photon confocal fluorescence microscope for imaging experiments. The fluorescence optical density was analyzed with ImageJ2x software (n = 3/group).

Antioxidant evaluation

Untreated RAW 264.7 cells were plated overnight in 24-well culture dishes without tissue culture treatment and treated with LPS (1 μg/ml) with or without Lys, AuNPs, and FLA. This was continued for 12 h and stimulated with MSU crystals (200 μg/ml) for 12 h. The glutathione (GSH), Superoxide dismutase-like enzyme (SOD-like enzyme), malondialdehyde (MAD), and ROS levels were assessed using GSH, SOD-like enzyme, MDA, and ROS assay kits (Solebro, Beijing, China), respectively, following the manufacturer's scheme (N≥3/group).

Hematoxylin-eosin staining

The ankle joints of anesthetized rat were fixed in buffered 4% PFA for 24 h and decalcified in 10% nitric acid + equal volume fixative for 3 days. Finally, they were embedded in paraffin, sliced, and stained with

hematoxylin and eosin (HE) (n=3/group). SD rats (180 g-220 g) were divided into four groups, and then different doses of FLA were injected intraperitoneally: control. After 30 days, the tissues (heart, kidney, liver, spleen, lung) were histologically analyzed by H&E staining (n = 3/group).

Target evaluation

Gout rat were randomly divided into the Sham group, model group, and FLA group. At the set time points (2, 4, 6, 12, and 24 h), the heart, liver, spleen, lung, kidney, and ankle of anesthetized rat were taken. And use IVIS Spectrum, PerkinElmer system to record the fluorescence distribution (n = 3/group).

Swelling assessment

30 minutes after intraperitoneal injection of MSU into the ankle joint cavity, MSU crystals or FLA (5 mg/kg, 10 mg/kg, 20 mg/kg) were intraperitoneally injected into the ankle joint cavity. A soft ruler was used to measure the ankle edema. By subtracting the initial circumference from the ankle joint circumference measured at each time point, the ankle joint edema of each mouse was determined and expressed as Δmm/joint (n = 3/group).

Inflammation and functional disorder evaluation

The classification criteria of inflammatory and dysfunctional indices are referred to the method according to the reference [31]. Grade 0 inflammatory index evaluation: normal; Grade 1: visible erythema, mild swelling, and bone signs; Grade 2: obvious redness and disappearance of bone signs, but the swelling is confined to the joints; Grade 3: swelling of the lateral limbs of the left-hand joint. Grade 0 dysfunction index evaluation: normal gait, all four feet are evenly on the ground; grade 1: left foot relaxed, toes open, mild lameness; grade 2: left hind foot bent, toes touched on the ground, obviously lame; grade 3: left hind foot completely off the land.

Statistical Analysis

All values are expressed as mean ± SEM. In the case of multiple comparisons, we used one-way ANOVA followed by Bonferroni post hoc test in case of equal variance and Kruskal-Wallis test in case of uneven variance. Ankle swelling function disorder index and inflammation index were analyzed using two-way ANOVA and Tukey post hoc test. $p < 0.05$ was considered to be statistically significant.

Abbreviations

FA: folic acid, Lys: modified lysozyme, AuNCs: gold nanoclusters, MSU:monosodium urate , FLA:folic acid -modified lysozyme -protected gold nanoclusters, Ros:reactive oxygen species , TEM:Transmission electron microscopy , ICP-MS:inductively coupled plasma mass spectrometry, EDC:1-ethyl-3-(-3-dimethylaminopropyl) carbodiimide, NHS:N-(3-Dimethylaminopropyl)-N'-ethyl carbodiimide hydrochloride , AuNPs: Gold nanoparticles

Declarations

Ethics approval and consent to participate

The experimental method was approved by the Animal Protection and Use Committee of Jinzhou Medical University. The animal data were reported following the ARRIVE 2.0 guidelines.ethical committee number:2021101.

Consent for publication

Not applicable.

Declaration of competing interest

The authors declare no conflicts of interest.

Availability of data and materials

The datasets used and/or analysed during the current study are available from the corresponding author on reasonable request.

Acknowledgments

We gratefully thank all colleagues who participated in this experiment.This work was supported by the Liaoning Revitalization Talents Program(NO. XLYC2002037) and Liaoning Revitalization Talents Program (NO. XLYC1902108).

Funding

This work was supported by the Liaoning Revitalization Talents Program(NO. XLYC2002037) and Liaoning Revitalization Talents Program (NO. XLYC1902108).

Authors' contributions

The experiment was completed with the help of multiple authors.Jiachen Sun wrote the main manuscript. Pengfei Zhuang provided technical support. Shan Wen, Minghao Ge,collected samples, ZiPeng Zhou data analysis. Xifan Mei, Chang Liu, Dan Li designed experiments and revised manuscripts. All authors read and approved the manuscript.

Appendix A. Supplementary materia

The following are the Supplementary data to this article:

References

[1]. Dalbeth N, Gosling AL, Gaffo A, Abhishek A. Gout. The Lancet. 2021;397(10287):1843-55.

[2]. Dalbeth N, Choi HK, Joosten LAB, Khanna PP, Matsuo H, Perez-Ruiz F, et al. Gout. Nat Rev Dis Primers. 2019;5(1):69.

[3]. Dalbeth N, Merriman TR, Stamp LK. Gout. The Lancet. 2016;388(10055):2039-52.

[4]. Drug, Therapeutics B. Latest guidance on the management of gout. BMJ. 2018;362:k2893.

[5]. Wehling P, Evans C, Wehling J, Maixner W. Effectiveness of intra-articular therapies in osteoarthritis: a literature review. Ther Adv Musculoskelet Dis. 2017;9(8):183-96.

[6]. Wang Q, Jiang H, Li Y, Chen W, Li H, Peng K, et al. Targeting NF-kB signaling with polymeric hybrid micelles that co-deliver siRNA and dexamethasone for arthritis therapy. Biomaterials. 2017;122:10-22.

[7]. Shin JM, Kim SH, Thambi T, You DG, Jeon J, Lee JO, et al. A hyaluronic acid-methotrexate conjugate for targeted therapy of rheumatoid arthritis. Chem Commun (Camb). 2014;50(57):7632-5.

[8]. Li R, He Y, Zhu Y, Jiang L, Zhang S, Qin J, et al. Route to Rheumatoid Arthritis by Macrophage-Derived Microvesicle-Coated Nanoparticles. Nano Lett. 2019;19(1):124-34.

[9]. Bolanos K, Kogan MJ, Araya E. Capping gold nanoparticles with albumin to improve their biomedical properties. Int J Nanomedicine. 2019;14:6387-406.

[10]. Kiyani MM, Rehman H, Hussain MA, Jahan S, Afzal M, Nawaz I, et al. Inhibition of Hyperuricemia and Gouty Arthritis in BALB/c Mice Using Copper Oxide Nanoparticles. Biol Trace Elem Res. 2020;193(2):494-501.

[11]. Kiyani MM, Butt MA, Rehman H, Ali H, Hussain SA, Obaid S, et al. Antioxidant and anti-gout effects of orally administered zinc oxide nanoparticles in gouty mice. J Trace Elem Med Biol. 2019;56:169-77.

[12]. Liu Y, Zhu H, Zhou W, Ye Q. Anti-inflammatory and anti-gouty-arthritic effect of free Ginsenoside Rb1 and nano Ginsenoside Rb1 against MSU induced gouty arthritis in experimental animals. Chem Biol Interact. 2020;332:109285.

[13]. Yuan Q, Wang Y, Zhao L, Liu R, Gao F, Gao L, et al. Peptide protected gold clusters: chemical synthesis and biomedical applications. Nanoscale. 2016;8(24):12095-104.

[14]. Zheng Y, Lai L, Liu W, Jiang H, Wang X. Recent advances in biomedical applications of fluorescent gold nanoclusters. Adv Colloid Interface Sci. 2017;242:1-16.

[15]. Xiao L, Wei F, Zhou Y, Anderson GJ, Frazer DM, Lim YC, et al. Dihydrolipoic Acid-Gold Nanoclusters Regulate Microglial Polarization and Have the Potential To Alter Neurogenesis. Nano Lett. 2020;20(1):478-95.

[16]. Wang J, Chang Y, Wu WB, Zhang P, Lie SQ, Huang CZ. Label-free and selective sensing of uric acid with gold nanoclusters as optical probe. Talanta. 2016;152:314-20.

[17]. Yang C, Gao S, Kjems J. Folic acid conjugated chitosan for targeted delivery of siRNA to activated macrophages in vitro and in vivo. J Mater Chem B. 2014;2(48):8608-15.

[18]. Chen D, Li J. Ultrasmall Au nanoclusters for bioanalytical and biomedical applications: the undisclosed and neglected roles of ligands in determining the nanoclusters' catalytic activities. Nanoscale Horiz. 2020;5(10):1355-67.

[19]. Yang Y, Guo L, Wang Z, Liu P, Liu X, Ding J, et al. Targeted silver nanoparticles for rheumatoid arthritis therapy via macrophage apoptosis and Re-polarization. Biomaterials. 2021;264:120390.

[20]. Zhao L, Jiang D, Cai Y, Ji X, Xie R, Yang W. Tuning the size of gold nanoparticles in the citrate reduction by chloride ions. Nanoscale. 2012;4(16):5071-6.

[21]. Trott O, Olson AJ. AutoDock Vina: improving the speed and accuracy of docking with a new scoring function, efficient optimization, and multithreading. J Comput Chem. 2010;31(2):455-61.

[22]. Wei H, Wang Z, Zhang J, House S, Gao YG, Yang L, et al. Time-dependent, protein-directed growth of gold nanoparticles within a single crystal of lysozyme. Nat Nanotechnol. 2011;6(2):93-7.

[23]. Kumar V, Chichili VP, Tang X, Sivaraman J. A novel trans conformation of ligand-free calmodulin. PLoS One. 2013;8(1):e54834.

[24]. Percie du Sert N, Hurst V, Ahluwalia A, Alam S, Avey MT, Baker M, et al. The ARRIVE guidelines 2.0: Updated guidelines for reporting animal research. PLoS Biol. 2020;18(7):e3000410.

[25]. Liu HJ, Pan XX, Liu BQ, Gui X, Hu L, Jiang CY, et al. Grape seed-derived procyanidins alleviate gout pain via NLRP3 inflammasome suppression. J Neuroinflammation. 2017;14(1):74.

[26]. Raucci F, Iqbal AJ, Saviano A, Minosi P, Piccolo M, Irace C, et al. IL-17A neutralizing antibody regulates monosodium urate crystal-induced gouty inflammation. Pharmacol Res. 2019;147:104351.

[27]. Liu L, Zhu X, Zhao T, Yu Y, Xue Y, Zou H. Sirt1 ameliorates monosodium urate crystal-induced inflammation by altering macrophage polarization via the PI3K/Akt/STAT6 pathway. Rheumatology (Oxford). 2019;58(9):1674-83.

[28]. Goldberg EL, Asher JL, Molony RD, Shaw AC, Zeiss CJ, Wang C, et al. beta-Hydroxybutyrate Deactivates Neutrophil NLRP3 Inflammasome to Relieve Gout Flares. Cell Rep. 2017;18(9):2077-87.

[29]. Martillo MA, Nazzal L, Crittenden DB. The crystallization of monosodium urate. Curr Rheumatol Rep. 2014;16(2):400.

[30]. Li H, Jiang W, Ye S, Zhou M, Liu C, Yang X, et al. P2Y14 receptor has a critical role in acute gouty arthritis by regulating pyroptosis of macrophages. Cell Death Dis. 2020;11(5):394.

[31]. Coderre TJ, Wall PD. Ankle joint urate arthritis (AJUA) in rats: an alternative animal model of arthritis to that produced by Freund's adjuvant. Pain. 1987;28(3):379-93.

[32]. Khan MA, Khan MJ. Nano-gold displayed anti-inflammatory property via NF-kB pathways by suppressing COX-2 activity. Artif Cells Nanomed Biotechnol. 2018;46(sup1):1149-58.

[33]. Martinon F, Petrilli V, Mayor A, Tardivel A, Tschopp J. Gout-associated uric acid crystals activate the NALP3 inflammasome. Nature. 2006;440(7081):237-41.

[34]. So A, Dumusc A, Nasi S. The role of IL-1 in gout: from bench to bedside. Rheumatology (Oxford). 2018;57(suppl_1):i12-i9.

[35]. Dinarello CA. Interleukin-1 in the pathogenesis and treatment of inflammatory diseases. Blood. 2011;117(14):3720-32.

[36]. Hall CJ, Sanderson LE, Lawrence LM, Pool B, van der Kroef M, Ashimbayeva E, et al. Blocking fatty acid-fueled mROS production within macrophages alleviates acute gouty inflammation. J Clin Invest. 2018;128(5):1752-71.

[37]. Ma Y, Tang T, Sheng L, Wang Z, Tao H, Zhang Q, et al. Aloin suppresses lipopolysaccharideinduced inflammation by inhibiting JAK1STAT1/3 activation and ROS production in RAW264.7 cells. Int J Mol Med. 2018;42(4):1925-34.

[38]. Bagheri M, Nair RR, Singh KK, Saini DK. ATM-ROS-iNOS axis regulates nitric oxide mediated cellular senescence. Biochim Biophys Acta Mol Cell Res. 2017;1864(1):177-90.

[39]. Huang Y, Li W, Su ZY, Kong AN. The complexity of the Nrf2 pathway: beyond the antioxidant response. J Nutr Biochem. 2015;26(12):1401-13.

[40]. Huang TT, Hao DL, Wu BN, Mao LL, Zhang J. Uric acid demonstrates neuroprotective effect on Parkinson's disease mice through Nrf2-ARE signaling pathway. Biochem Biophys Res Commun. 2017;493(4):1443-9.

[41]. Li K, Li D, Li CH, Zhuang P, Dai C, Hu X, et al. Efficient in vivo wound healing using noble metal nanoclusters. Nanoscale. 2021;13(13):6531-7.

[42]. Zhang K, Zeng X, Chen Y, Zhao R, Wang H, Wu J. Therapeutic effects of Qian-Yu decoction and its three extracts on carrageenan-induced chronic prostatitis/chronic pelvic pain syndrome in rats. BMC Complement Altern Med. 2017;17(1):75.

Figures

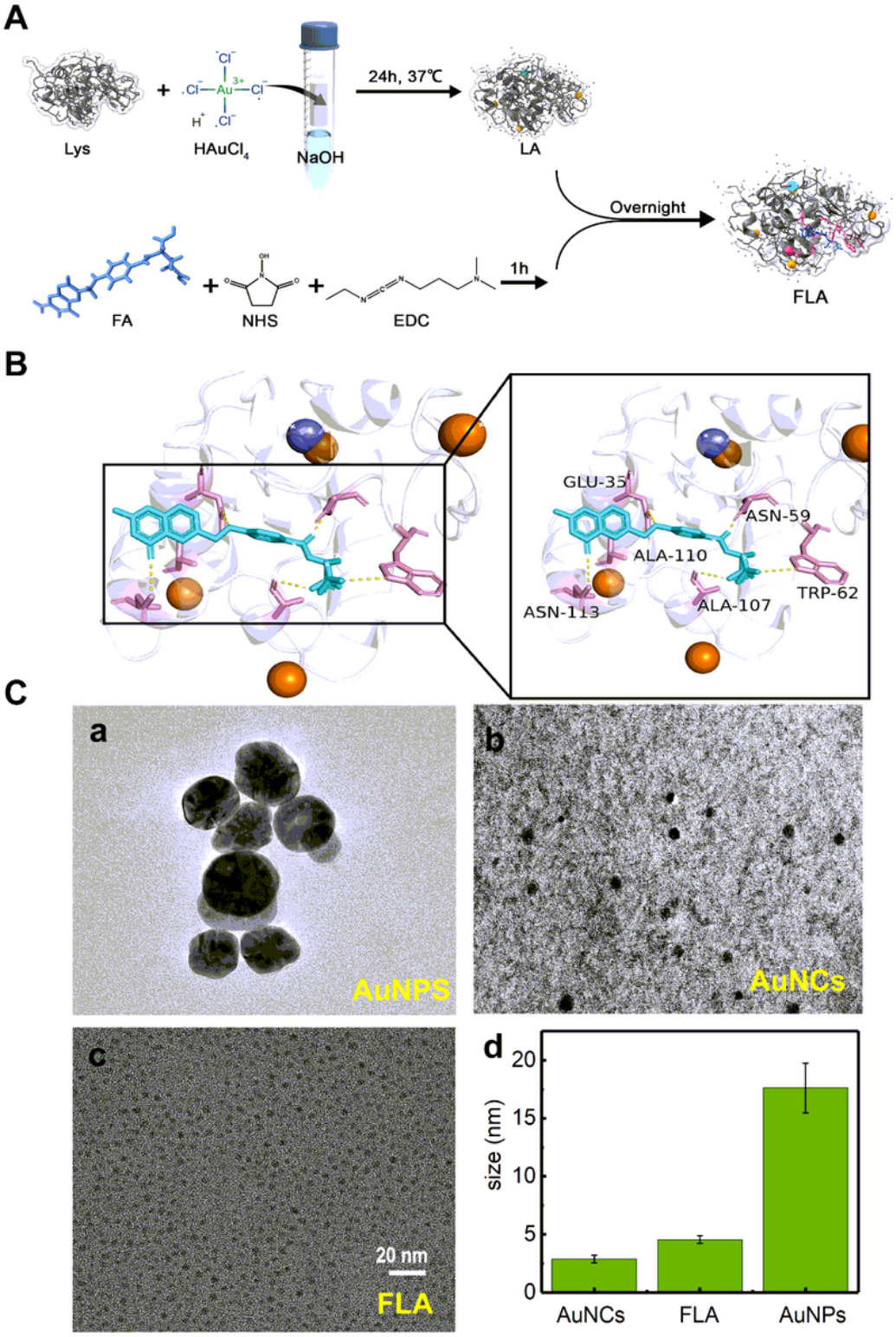

Figure 1

Scheme for fabrication of FLA (A); The molecular docking for the stabilized ligand (Lys) of AuNCs and folic acid (FA) (B); TEM of AuNCs (also noted as LA) (a), FLA (b), AuNPs (c) and their average sizes (d).

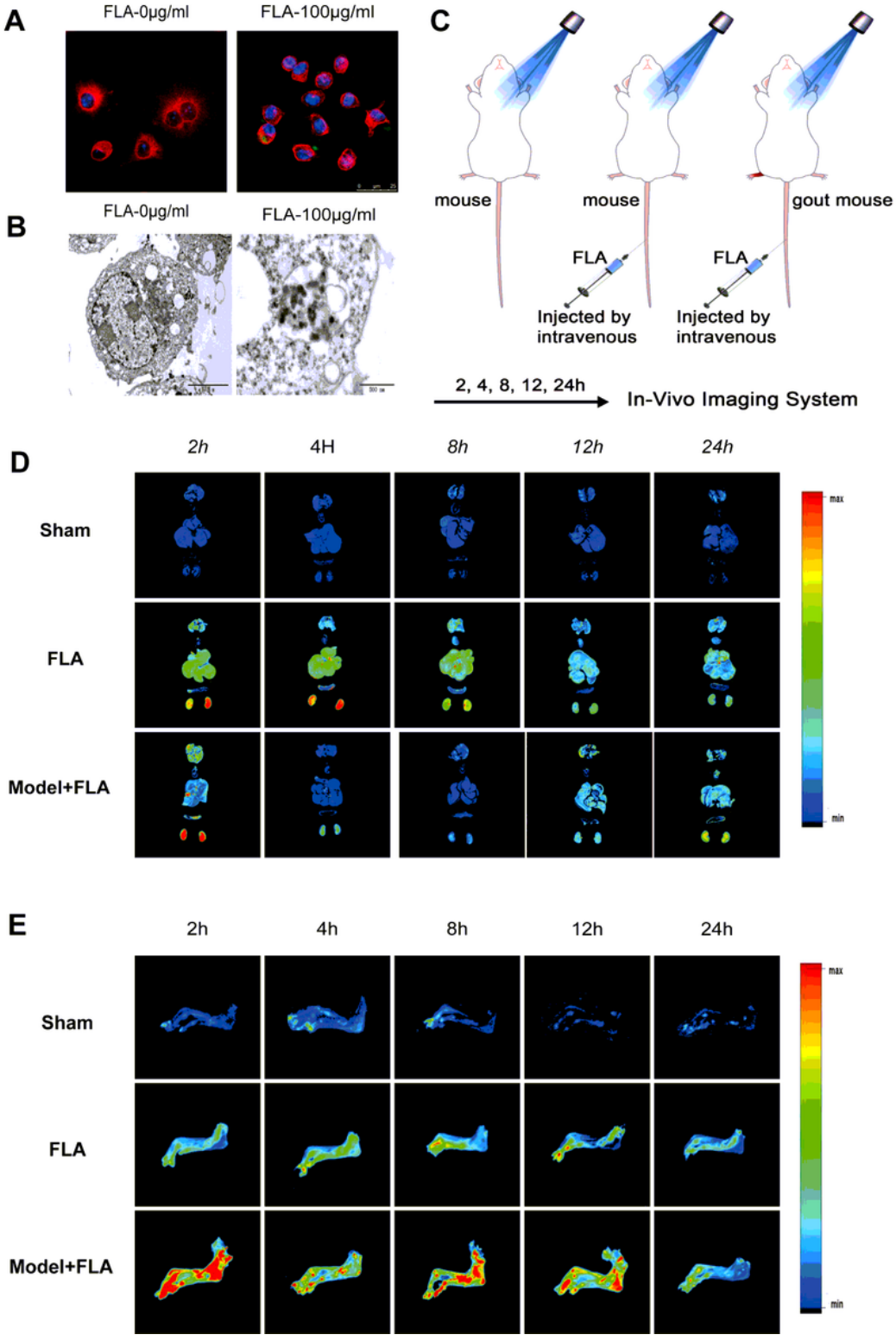

Figure 2

Raw 264.7 cells treated with 100 μM of FLA after 24 h and observed by single-photon confocal microscopy (A). Raw 264.7 cells treated with 100 μM FLA after 24 h and observed by TEM; Scale bar = 5μM (B). Flow chart of joint imaging of live rat (C). Fluorescence images of the heart, liver, spleen, lungs, and kidneys of normal rat, FLA-injected normal rat, and FLA-injected gout rat from 2 to 24 h after injection. Scale bars are used for fluorescence signal counting (D). Fluorescence images of the ankle of

normal rat, FLA-injected normal rat, and FLA-injected gout rat from 2 to 24 h after injection. Scale bars are used for fluorescence signal counting (E).

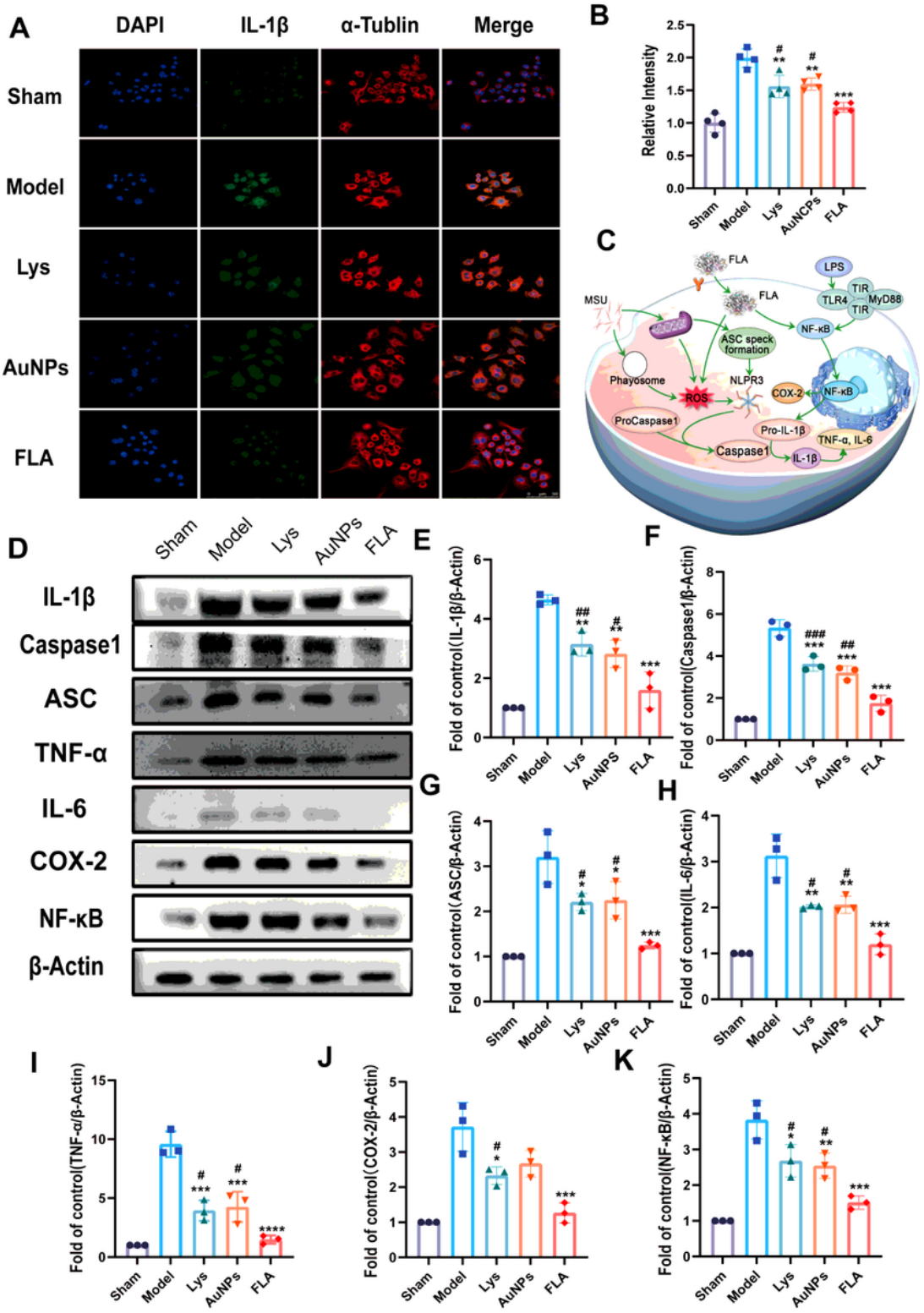

Figure 3

The effects of different agents on Raw 246.7 cells (A). Immunofluorescence intensity analysis of IL-1β in Raw 246.7 cell culture (n=3/group) (B). Schematic representation of FLA inhibition of IL-1β production in RAW 264.7 cell cultures (C). Inhibition of IL-1β, Caspase1, ASC, COX-2, IL-6, TNF-α, NF-κB by Lys, AuNPs,

FLA in LPS and MSU stimulated RAW 246.7 cells by Western blot analysis (D). Western blotting detection of IL-1β (E) Caspase1 (F) ASC (G) IL-6 (H) TNF-α(I) COX-2 (J) NF-κB (K) inflammation-associated protein expression in Raw 264.7 cell cultures in each group (n=3/group). * compared with Model group, # compared with FLA group, data expressed as mean ± SD, * $p < 0.05$, ** $p < 0.01$ *** $p < 0.001$ ****$p < 0.0001$.

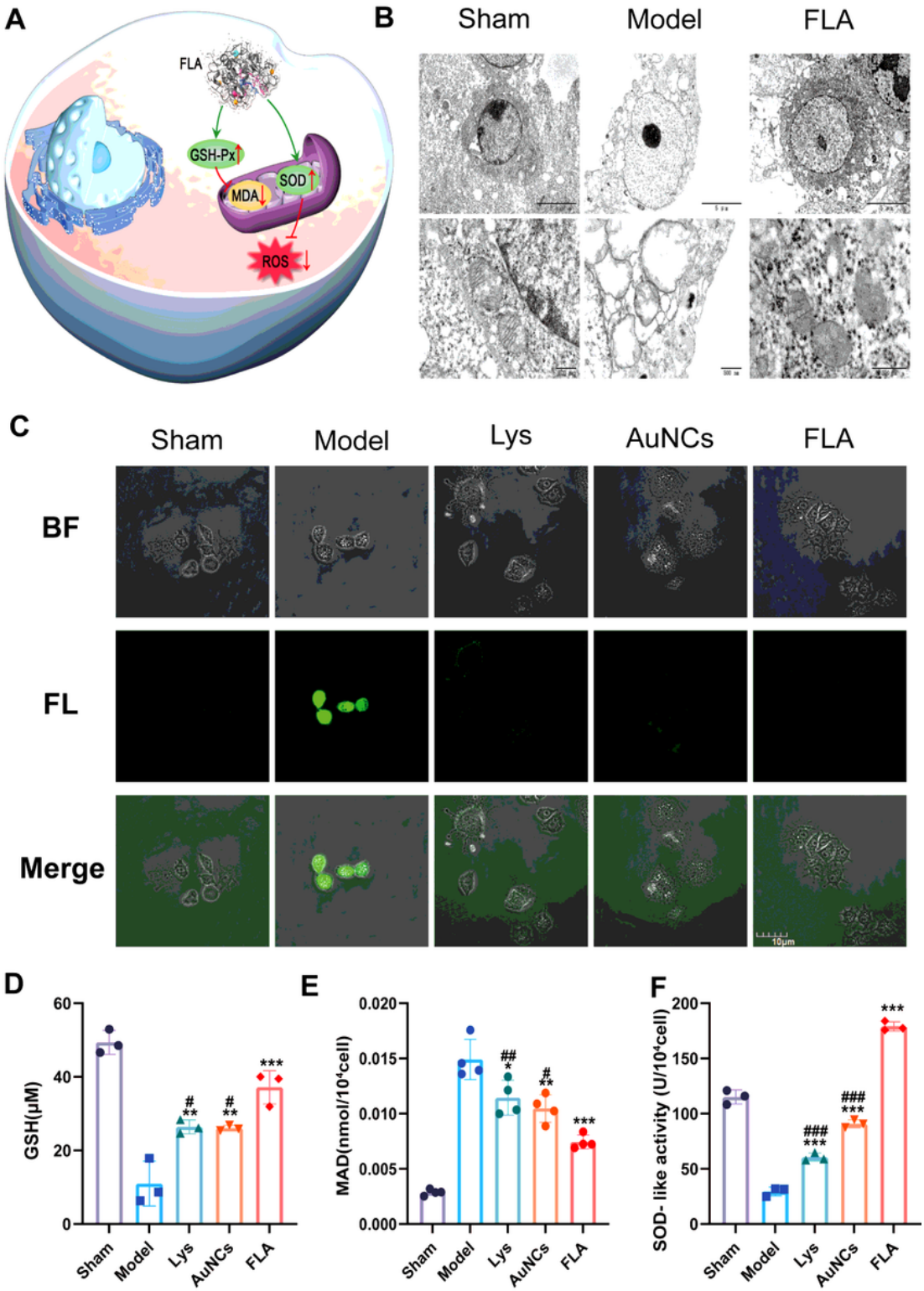

Figure 4

Schematic diagram of FLA reducing ROS production in Raw 246.7 cells (A). Cell morphology and mitochondrial morphology of each group under TEM; Sclar bar = 5 μM (up) and 500 nm (below) (B). ROS production was observed in different groups of Raw 246.7 cells under fluorescence microscopy at a magnification of 600 times. ROS formation was most significantly inhibited in the FLA-treated group based on the completely quenching of the fluorescence of the ROS probe (n = 3) (C). SOD-like activity of the agents on Raw 246.7 cells (n ≥ 3/group) (D). MDA concentrations in Raw 246.7 cells of each group (E). GSH content in Raw 246.7 cells of each group (F). Data are expressed as mean ± SD, * $p < 0.05$, ** $p < 0.01$ *** $p < 0.001$ ****$p < 0.0001$ compared to vs. Model. # $p < 0.05$, ## $p < 0.01$, ### $p < 0.001$, #### $p < 0.0001$ compared to the control group.

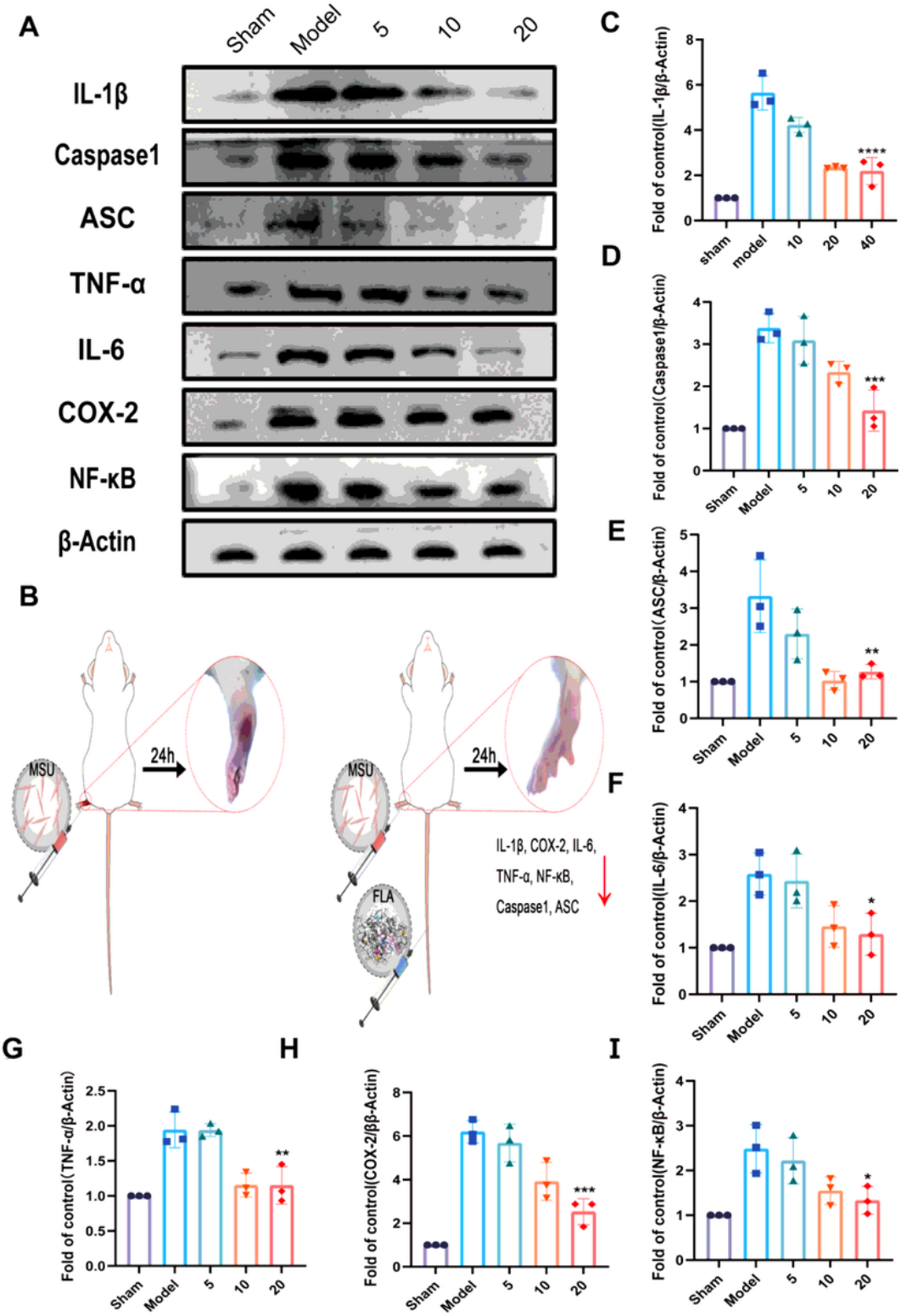

Figure 5

Inhibition of IL-1β, Caspase1, ASC, COX-2, IL-6, TNF-α, NF-kB in the ankle of SD rats injected with MSU by protein concentration blotting of different concentrations of FLA (A). Schematic representation of FLA inhibition of IL-1β in mouse ankle homogenates (B). Western blotting to detect the expression of IL-1β (C) Caspase1 (D) ASC (E) IL-6 (F) TNF-α (G) COX-2 (H) NF-κB (I) inflammation-related proteins in the ankle

homogenates of rat in each group (n=3/group). Data are expressed as mean ± SD, * p < 0.05, ** p < 0.01, *** p < 0.001, **** p < 0.0001 compared to control.

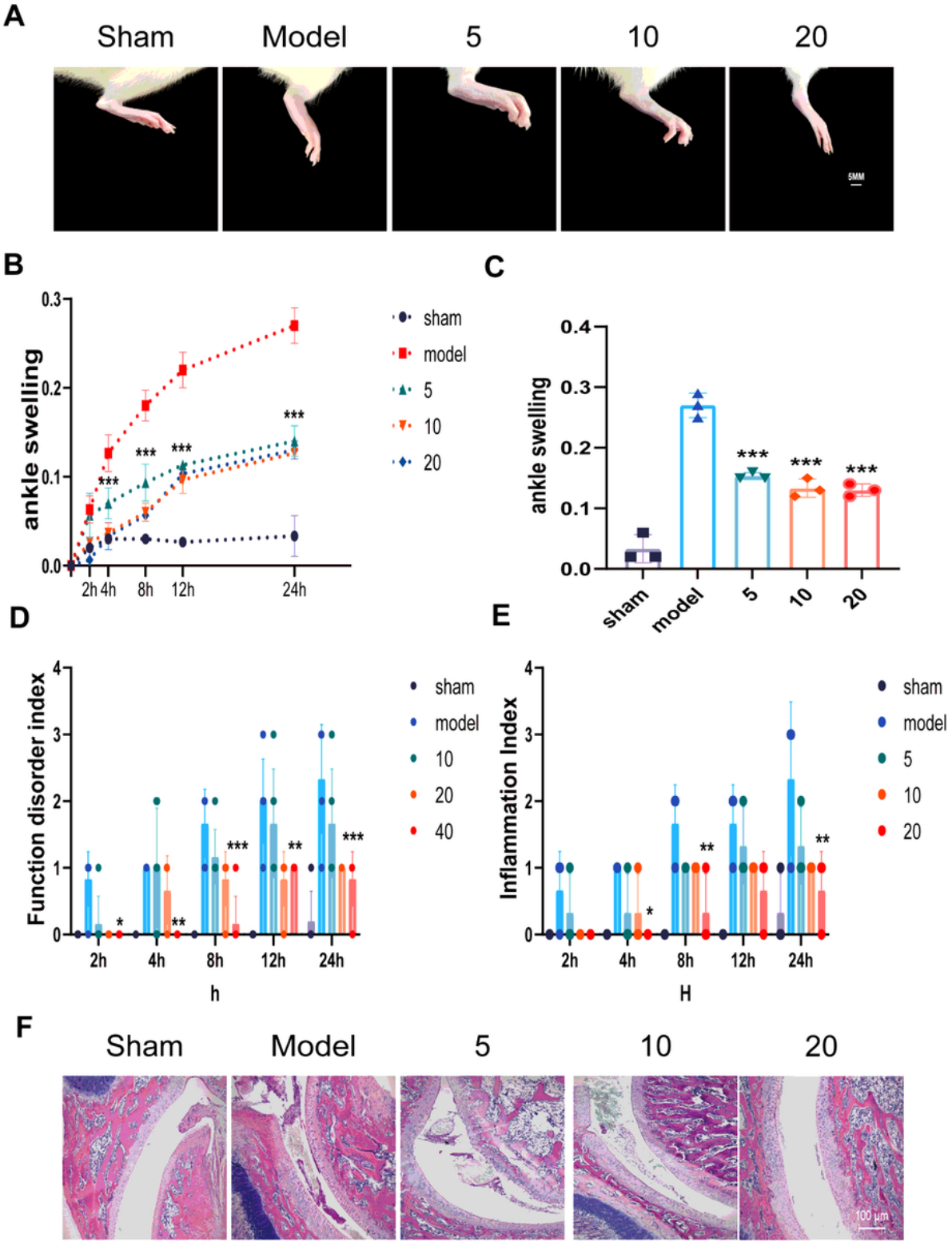

Figure 6

Representative photographs of the ankle joints of rat 24 h after MSU crystal injection (A). Time course of MSU-induced changes in ankle swelling (n=3) (B). 24h swelling of the ankle caused by MSU (C). Practice course of MSU crystal-induced changes in ankle joint function disorder index and (n=3) (D). Practice

course of MSU crystal-induced changes in ankle joint inflammation index and (n=3) (E). Hematoxylin and eosin-stained sections of the ankle joint were obtained 24 h after injection (n=3) (F). Data are expressed as mean ± SD, * $p < 0.05$, ** $p < 0.01$, *** $p < 0.001$, ****$p < 0.0001$ compared with Model group.

Supplementary Files

This is a list of supplementary files associated with this preprint. Click to download.

- SupplementaryMaterial.docx
- Graphicalabstract.tif